International Journal of Modern Physics E
Vol. 26 (2017) 1750012 (24 pages)

DOI: 10.1142/S0218301317500124

RPA treatment of a motivated QCD Hamiltonian in the SO(4) (2+1)-flavor limit: Light and strange mesons

Tochtli Yepez-Martinez*,‡, Osvaldo Civitarese*,§
and Peter O. Hess†,¶

*Departamento de Fisica,
Universidad Nacional de La Plata,
C.C.67 (1900), La Plata, Argentina

†Instituto de Ciencias Nucleares,
Universidad Nacional Autónoma de México,
Ciudad Universitaria, Circuito Exterior S/N,
A.P. 70-543, 04510 México D. F. México

‡yepez@fisica.unlp.edu.ar
§osvaldo.civitarese@fisica.unlp.edu.ar
¶hess@nucleares.unam.mx

Received 8 November 2016
Revised 10 January 2017
Accepted 20 January 2017
Published 16 February 2017

The SO(4) symmetry of a sector of the quantum chromodynamics (QCD) Hamiltonian was analyzed in a previous work. The numerical calculations were then restricted to a particle–hole (ph) space and the comparison with experimental data was reasonable in spite of the complexity of the QCD spectrum at low energy. Here on, we continue along this line of research and show our new results of the treatment of the QCD Hamiltonian in the SO(4) representation, including ground state correlations by means of the Random Phase Approximation (RPA). We are able to identify, within this model, states which may be associated to physical pseudo-scalar and vector mesons, like $\eta, \eta', K, \rho, \omega, \phi$, as well as the pion ($\pi$).

Keywords: SO(4) symmetries; effective QCD Hamiltonian; RPA; many body aspects of mesons.

PACS Number(s): 12.38.−t, 12.40.Yx, 21.60.Fw, 14.40.−n

1. Introduction

Although quantum chromodynamics (QCD) is a well established theory of the strong interactions, its realization in the low-energy regime is a very difficult task which until now has not been satisfactorily completed. Part of the difficulties of low-energy QCD is due to the nonperturbative nature of the theory, which invalidates

§Corresponding author.

the use of standard perturbative methods of calculations in field theory.[1–3] Other potential difficulties are the uncertainties in the correct identification of physical degrees of freedom "starting" from the elementary fields of the theory, i.e., the origin of confinement in color degrees of freedom,[4,5] the competition between valence-quarks, sea-quarks and gluonic excitations.[6–10]

Several methods are available to treat QCD in its nonperturbative regime. Among them, Dyson–Schwinger-type of expansions, which start from quark and gluon propagators at tree-level, leading to effective potentials,[11–14] and Lattice QCD (LQCD) calculations,[4,9,15–20] which consist of a discretization of the dynamical fields of the theory, have provided significant advances in nonperturbative aspects of the fundamental theory of strong interactions. Out of them, LQCD is the best formalism which can handle QCD from first principles but its numerical implementation is quite involved. On the other hand, fixing-gauge approaches, like the canonical Coulomb gauge,[1,5,21–27] offers a connection between QCD and the nonrelativistic many-body problem in nuclear physics. However, the full effects of quark–antiquark pairs have never been considered because such effects lead to a many-body problem that can only be treated in some phenomenological approximations. These kinds of models are of interest to illuminate possible connections between phenomenological models and QCD.

In a previous work,[28] we have shown that a sector of the QCD Hamiltonian in the canonical Coulomb gauge representation,[1,5] exhibits a SO(4) symmetry in a reduced configurational space. From this point, we shall refer to it as an effective QCD inspired Hamiltonian suitable to describe light and strange mesonic excitations. Starting from the generators of the SO(4) group, we have replaced a sector of the QCD Hamiltonian by a linear combination of the Casimir operators of the SO(4) group. Then, we have worked with its analytic solution and given to it a physical interpretation in terms of the available data on $J^\pi = 0^-, 1^-$ meson states. After that we have partially broken the SO(4) symmetry, enlarging the basis in order to include particle–hole (ph) excitations and applied the Tamm–Dancoff Approximation (TDA) to extract the energies and wave functions.

In this work, we continue with this line of approach by considering a larger space in order to include ground state correlations. We have adopted the Random Phase Approximation (RPA),[29] which is a well-known technique in other fields of physics like: nuclear physics, solid state physics, atomic physics, etc. It is basically a harmonic oscillator representation which treats fluctuations around a mean field as superpositions of one and two ph states. In the present context, we aim at the description of mesonic states as RPA-phonon states. To perform a more realistic analysis from the physical point of view, we have also added the flavor degree of freedom and endowed the single particle states of the basis with a flavor dependence.

The paper is organized as follows. In Sec. 2, we introduce the QCD Hamiltonian in the Coulomb gauge and extract from it an effective Hamiltonian which includes

confinement. Then, in Sec. 3, we write the quantized expression for the effective Hamiltonian in term of creation and annihilation operators. We perform a mapping of the quantized effective QCD Hamiltonian onto the SO(4) representations. In the same section, we extend the SO(4)-scheme of Ref. 28 to include flavor degrees of freedom. The details of the RPA method and its implementation in the present study are presented at the end of Sec. 3. In Sec. 4, we resume and discuss the results of the calculations. We focus on the correspondence between calculated and physical states and discuss the role of the masses in the calculations. Finally, we summarize our conclusions in Sec. 5.

2. Canonical QCD Coulomb Gauge Hamiltonian

The fundamental non-abelian theory of strong interactions, QCD, has been widely studied in its canonical Coulomb gauge representation.[1,5,22] It was shown in Ref. 5 that two of the main features of QCD, e.g., confinement and the constituent particles (quarks and gluons) can be treated simultaneously in that framework. The QCD Hamiltonian, in the canonical Coulomb gauge representation is written as

$$\begin{aligned} H^{\rm QCD} = & \int \Big\{ \frac{1}{2}[\mathcal{J}^{-1}\Pi_i^{tr\,a}\mathcal{J}\Pi_i^{tr\,a} + \mathcal{B}_i^a\mathcal{B}_i^a] \\ & - \overline{\psi}_{cf}(-i\gamma\cdot\nabla + m)\psi_{cf} - g\overline{\psi}_{cf}\gamma\cdot A^a T^a_{cc'}\psi_{c'f} \Big\} d\mathbf{r} \\ & + \frac{1}{2}g^2 \int \mathcal{J}^{-1}\rho^a(\mathbf{r}) \left\langle a,\mathbf{r} \left| \frac{1}{\nabla\cdot\mathcal{D}}(-\nabla^2)\frac{1}{\nabla\cdot\mathcal{D}} \right| a'\mathbf{r}' \right\rangle \mathcal{J}\rho^{a'}(\mathbf{r}')d\mathbf{r}d\mathbf{r}'. \end{aligned} \quad (1)$$

The transverse chromo-electromagnetic fields in QCD Coulomb gauge are indicated by Π and $\mathcal{B}$, while ψ represents the quark fields. The last two-terms in Eq. (1) are the quark–gluon interaction (g-term) and the quark (anti-quark) ($\rho(\mathbf{r})$) color charge-density interaction (g^2-term), respectively. The latter is a gauge-dependent interaction coming from the inverse of the Faddeev–Popov term, $(\nabla\cdot\mathcal{D})^{-1}$, and its determinant $\mathcal{J} = \det(\nabla\cdot\mathcal{D})$.[1] In the low-energy regime of QCD, light quarks and their interactions play the most important role and the effects of dynamical gluons may be absorbed in the interaction $V(R) = -\frac{\alpha}{R} + \beta R$, which is obtained from a self-consistent treatment of the gauge-dependent interaction between color charge densities, as it was shown in Ref. 5. Therefore, one can write for the effective QCD Hamiltonian the expression

$$H^{\rm QCD}_{\rm eff} = \int \{\psi^\dagger(\mathbf{r})(-i\alpha\cdot\nabla + \beta m)\psi(\mathbf{r})\}d\mathbf{r} + \frac{1}{2}\int \rho_a(\mathbf{r})V(|\mathbf{r}-\mathbf{r}'|)\rho^a(\mathbf{r}')d\mathbf{r}d\mathbf{r}', \quad (2)$$

where $\rho^a(\mathbf{r}) = \rho^a_q(\mathbf{r}) + \rho^a_{\bar{q}}(\mathbf{r}) = \psi^\dagger(\mathbf{r})T^a\psi(\mathbf{r})$ and $\psi^\dagger(\mathbf{r}) = (\psi^\dagger_1(\mathbf{r},\sigma,c,f), \psi^\dagger_2(\mathbf{r},\sigma,c,f))$ with σ, c, f indicating the spin, color and flavor intrinsic degrees of freedom.

Concerning the spectrum of low-energy mesons LQCD[9,20] and many-body techniques have been applied, mostly numerically, to reproduce certain characteristics of the spectrum. Practically, all those approaches fail in reproducing the pion mass.

Some of the standard bosonization-methods, like the TDA and RPA, have shown to be useful[30] to elucidate the role of the pion as a Goldstone-like state of the theory. Although the many-body methods are much less involved than lattice calculations, their implementation, requires some minimal information, i.e., about quarks masses, couplings and interactions, the fundamental degrees of freedom and about the symmetries exhibited by them.

3. The SO(4) Model Hamiltonian and its RPA Treatment

The motivation of this work comes from the side of the effective QCD Hamiltonian, Eq. (2), and the predictive power of nonperturbative many-body methods for the low-energy regime of QCD. In particular, the π, η and η' states seem to be a good laboratory for testing the many-body-methods.[30]

The quantized structure of the effective Hamiltonian Eq. (2) has been discussed in Ref. 27 and its expression, amenable to TDA or RPA treatments, is given by

$$
\begin{aligned}
H_{\rm eff}^{\rm QCD} = & \sum_{\Gamma_1} \varepsilon_{\Gamma_1} (b^\dagger_{\Gamma_1\mu_1} b_{\Gamma_1\mu_1} - d_{\Gamma_1\mu_1} d^\dagger_{\Gamma_1\mu_1}) \\
& + \sum_{\Gamma} \sum_{\Gamma_i} \Big\{ V_1(\Gamma_i) [([b^\dagger_{\Gamma_1} \otimes b_{\Gamma_2}]^\Gamma \\
& - [d_{\Gamma_1} \otimes d^\dagger_{\Gamma_2}]^\Gamma) \otimes ([b^\dagger_{\Gamma_3} \otimes b_{\Gamma_4}]^\Gamma - [d_{\Gamma_3} \otimes d^\dagger_{\Gamma_4}]^\Gamma)]^{\hat{0}_J}_{\hat{0}_M} \\
& + V_4(\Gamma_i) [([b^\dagger_{\Gamma_1} \otimes d^\dagger_{\Gamma_2}]^\Gamma + [d_{\Gamma_1} \otimes b_{\Gamma_2}]^\Gamma) \otimes ([b^\dagger_{\Gamma_3} \otimes d^\dagger_{\Gamma_4}]^\Gamma \\
& + [d_{\Gamma_3} \otimes b_{\Gamma_4}]^\Gamma)]^{\hat{0}_J}_{\hat{0}_M} \Big\}. \qquad (3)
\end{aligned}
$$

In Eq. (3), $b^\dagger_{\Gamma_i\mu_i}(b_{\Gamma_i\mu_i})$ and $d^\dagger_{\Gamma_i\mu_i}(d_{\Gamma_i\mu_i})$ refer to the creation (annihilation) operator of quarks and anti-quarks, respectively. We have used the short-hand notation $\Gamma_i = \{j_i, (1,0), (1,0)\}$ and $\mu_i = \{m_i, c_i, f_i\}$ for the single particle irreducible representations (irreps) of spin, color and flavor quantum numbers and their magnetic projections, respectively. The intermediate couplings of spin, color and flavor are indicated by $[\otimes]^\Gamma$ with $\Gamma = \{L, (1,1), (0,0)\}$ and $L = 0, 1$.[25,27] The matrix elements, V_i, of a confining interaction (Coulomb plus linear potential) in the harmonic oscillator basis have been explicitly given in Ref. 27. The scalar character of the Hamiltonian in spin, color and flavor quantum numbers is represented by the symbol $[\cdots]^{\hat{0}_J}_{\hat{0}_M}$, where the upper index $\hat{0}_J$ is a short-hand notation for the irreps $\{0, (0,0), (0,0)\}$ and the lower index $\hat{0}_M$ indicates their magnetic projections $\{0,0,0\}$. The uncorrelated vacuum state is represented by $|\tilde{0}\rangle$ and it is annihilated by the action of $b_{\Gamma\mu}$, and $d_{\Gamma\mu}$, i.e., $b_{\Gamma\mu}|\tilde{0}\rangle = d_{\Gamma\mu}|\tilde{0}\rangle = 0$. In order to achieve basis independence of the observables (eigenvalues) from the diagonalization of the Hamiltonian of Eq. (3) the number of configurations $(\Gamma_i\mu_i)$ should be large, but a reduction of the Fock space may provide some insights on the low-energy spectrum of mesons. To achieve

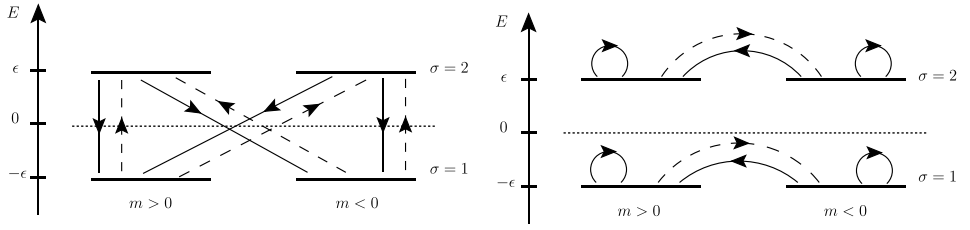

(a) (b)

Fig. 1. (a) Rising and lowering of the σ-value operations. (b) Invariant σ-value operations.

this goal, we have constructed all possible transition operators which are activated in the space depicted in Fig. 1.

The minimal model studied in Ref. 28 relies on the fact that physical states are color singlets and that the states were not classified by their flavor content since that requires the flavor symmetry to be explicitly broken. In Ref. 28, it was also shown that all the operations of Fig. 1 and the corresponding algebra are described by the SO(4) group. In Ref. 31, the SO(4) group algebra and its irreducible representations (j_0, η) have been widely analyzed.

The number of operations in this specific space is 16, and they are also shown in Fig. 1. Eight of these correspond to rising and lowering the value of σ and the other eight leave the value of σ invariant. The label σ is associated with anti-particle ($\sigma = 1$) and particle ($\sigma = 2$) states and m denotes the magnetic number of the particle (anti-particle) state. All the operations of the space shown in Fig. 1 are described by the action of the following six operators:

$$\begin{aligned}
\hat{J}_+ &= \sum_m C^\dagger_{2m} C_{1m}, \quad \hat{J}_- = \hat{J}^\dagger_+, \quad \hat{J}_0 = \sum_{\sigma,m} \frac{(-1)^\sigma}{2} C^\dagger_{\sigma m} C_{\sigma m}, \\
\hat{V}_+ &= \sum_m C^\dagger_{2m} C_{1-m}, \quad \hat{V}_- = \hat{V}^\dagger_+, \quad \hat{V}_0 = \sum_{\sigma,m} \frac{(-1)^\sigma}{2} C^\dagger_{\sigma m} C_{\sigma -m},
\end{aligned} \tag{4}$$

which are analogous to the operators appearing in the effective Hamiltonian of Eq. (3). This can be seen using the association $b^\dagger \to C^\dagger_2$ and $d^\dagger \to C_1$. Then, it is rather easy to identify the operators $\hat{J}_0$ and $\hat{V}_0$ with the transitions depicted in Fig. 1(b), while the operators $J_\pm$ and $V_\pm$ are to be associated to the transitions depicted in Figure 1(a). The commutators $[\hat{O}_1, \hat{O}_2]$ for the set of operators of Eq. (4) are given by[28]

$$\begin{aligned}
&[\hat{J}_\pm, \hat{J}_\mp] = \pm 2\hat{J}_0, \quad [\hat{V}_\pm, \hat{V}_\mp] = \pm 2\hat{J}_0, \quad [\hat{J}_\pm, \hat{V}_\mp] = \pm 2\hat{V}_0, \\
&[\hat{J}_0, \hat{J}_\pm] = \pm \hat{J}_\pm, \quad [\hat{V}_0, \hat{V}_\pm] = \pm \hat{J}_\pm, \quad [\hat{J}_0, \hat{V}_\pm] = \pm \hat{V}_\pm, \quad [\hat{V}_0, \hat{J}_\pm] = \pm \hat{V}_\pm,
\end{aligned} \tag{5}$$

and the two Casimir operators of the SO(4) group, $\hat{\mathcal{C}}_1$ and $\hat{\mathcal{C}}_2$, which commute with all the generators are given by

$$\begin{aligned}\hat{\mathcal{C}}_1 &= \hat{\mathbf{J}}^2 + \hat{\mathbf{V}}^2 = \hat{J}_+\hat{J}_- + \hat{V}_+\hat{V}_- + \hat{V}_0^2 + \hat{J}_0(\hat{J}_0 - 2),\\ \hat{\mathcal{C}}_2 &= \hat{\mathbf{J}}\cdot\hat{\mathbf{V}} = \frac{1}{2}(\hat{J}_-\hat{V}_+ + \hat{J}_+\hat{V}_-) + \hat{J}_0\hat{V}_0.\end{aligned} \tag{6}$$

Having identified the SO(4) group-operators within a sub-space of the quantized QCD-Coulomb-gauge Hamiltonian, we introduce a new Hamiltonian which maps the QCD Hamiltonian onto a combination of the two invariant SO(4) Casimir operators and theirs corresponding generators

$$H = 2\epsilon\hat{J}_0 + a_M\hat{\mathcal{C}}_1 + b_M\hat{\mathcal{C}}_2, \tag{7}$$

where the first term is the free Dirac term and a_M, b_M are the coupling constants of the model. A brief summary of the findings of our previous work, Ref. 28, is the following: (i) we have considered the possible SO(4)-irreps (j_0, η) that could be involved in the meson spectrum of Eq. (7), i.e., $(j_0, \eta) = (0, 1), (0, 2), (\pm 1, 2)$, (ii) a fit of the parameters to experimental meson states up to 1 GeV led to the values $\epsilon = 54.20\,\text{MeV}$, $a_M = 236.98\,\text{MeV}$ and $b_M = 15.82\,\text{MeV}$ and (iii) the SO(4) spectrum indicated that the physical states (J, M_J) may be contained in the SO(4) (j_0, η)-irreps, where we have identified the $(0, 1)$-irrep as a state of zero mass (Goldstone boson) which is independent of the parameters of the model. The other SO(4)-irreps $(0, 2)$ and $(\pm 1, 2)$ were located at average masses between the pseudo-scalar and vector meson masses.[28] To get a closer contact with the experimental energies may require additional corrections coming from, e.g., a more general interaction, the SU(3)-flavor symmetry breaking and vacuum-correlations, among others.

Taking the Casimir structure of Eq. (7) as the starting point, we have constructed a more general Hamiltonian for the space of Fig. 1. It reads

$$\begin{aligned}H = {} & 2(\epsilon - a_4)\hat{J}_0 - a_7\hat{V}_0 + a_2\hat{V}_0^2 + a_3\hat{J}_0^2 + a_6\hat{V}_0\hat{J}_0 + \frac{a_1}{2}(\hat{J}_+\hat{J}_- + \hat{V}_+\hat{V}_-)\\ & + \frac{a_5}{2}(\hat{J}_+\hat{V}_- + \hat{V}_-\hat{J}_+ + h.c.) + b((\hat{J}_+ + \hat{V}_+)(\hat{J}_+ + \hat{V}_+) + h.c.).\end{aligned} \tag{8}$$

In QCD, the gluon field carries spin and color intrinsic degrees of freedom, making the two-body interaction coefficients a's and b's spin and color dependent. When the effects of gluons are ignored the bilinear combinations $\hat{J}_i\hat{V}_j$ with $i, j = 0, \pm$ should be removed from the Hamiltonian of Eq. (8), since they are not scalars.

In this work, we leave open the possibility of more general or realistic interactions expected from QCD, motivated from its Coulomb gauge representation given in Eq. (1), and implement the RPA-method for a flavor-symmetry-breaking Hamiltonian (FSBH). From the QCD Hamiltonian, Eq. (1), it is easy to see that the simplest way to break the flavor symmetry is by the Dirac mass term. In our case, the ϵ-term is associated with the Dirac term and the a_4-term is associated explicitly with mass corrections coming from the two-body interactions. Therefore, since we

are going to work with effective masses (dressed or corrected by interactions), we replace the term $2(\epsilon - a_4)$ by a flavor dependent single particle term. In doing it we are explicitly breaking the chiral symmetry, as it will become evident from the values of the effective quark masses which we use in the calculations (see Sec. 4). We will use effective masses for light u, d and strange s quarks, whose values are in agreement with those introduced as running dynamical masses, near zero momentum in Ref. 30.

Therefore, we write the Hamiltonian in the following form:

$$\begin{aligned} H = & (\epsilon_f C^{\dagger}_{2m,f} C_{2m,f} - \epsilon_{f'} C^{\dagger}_{1m,f'} C_{1m,f'}) - a_7 \hat{V}_0 + a_2 \hat{V}_0^2 + a_3 \hat{J}_0^2 + a_6 \hat{V}_0 \hat{J}_0 \\ & + \frac{a_1}{2}(\hat{J}_+ \hat{J}_- + \hat{V}_+ \hat{V}_-) + \frac{a_5}{2}(\hat{J}_+ \hat{V}_- + \hat{V}_- \hat{J}_+ + h.c.) \\ & + b((\hat{J}_+ + \hat{V}_+)(\hat{J}_+ + \hat{V}_+) + h.c.). \end{aligned} \tag{9}$$

The ϵ_f-term takes into account the nonexact SU(3) flavor symmetry between the up, down and strange quarks. This should be relevant in order to make a better analysis of the structure of the spectrum in the low-energy regime.

The a_i coefficients associated to the bilinear combinations $J_+ J_-$ and $V_+ V_-$ in Eq. (9), play the role of scalar interactions associated to the creation-annihilation of pairs. The a_i coefficients associated to the bilinear combinations $J_\pm V_\mp$ and $J_0 V_0$ in Eq. (9), play the role of the interactions that take into account the gluonic degrees of freedom, in an effective way (e.g., a power expansion in gluon fields ($\mathbf{A}_i = \mathbf{A}_i^a T^a$),[1]) since these interactions require a spin transfer. The bilinear terms $J_\pm V_\mp$ and $J_0 V_0$ appear natural in the SO(4) invariant operators, Eq. (6), and can be associated with the power expansion in gluon fields of the inverse of the Faddeev–Popov term in Eq. (1). The a_7 coefficient associated to the one-body operator V_0 also accounts for the gluonic degrees of freedom in an effective way, since it plays the role of the quark–gluon interaction (g-term) in Eq. (1). The a_2 and a_3 coefficients associated to $\hat{V}_0^2$ and $\hat{J}_0^2$ respectively, play the role of number operators in the SO(4) group but the a_2-term is also capable of spin transfer. The b-coefficient associated to the two-body interactions, responsible of the creation and annihilation of two-pairs, accounts for the effects of the ground state correlations.

3.1. *RPA-method in the SO(4) model*

The details of the RPA-method are presented in Appendix A. The RPA-method, applied to the Hamiltonian of Eq. (9) yields the forward ($A_{a'b',ab}$) and backward ($B_{a'b',ab}$) matrices,[29]

$$\begin{aligned} A_{\alpha'\beta',\alpha\beta} = & \left\{ \epsilon_{f_\alpha} + \epsilon_{f_\beta} + 2a_1 + \frac{a_2}{2} + a_3 \right\} \delta_{m_{\alpha'},m_\alpha} \delta_{m_{\beta'},m_\beta} \delta_{f_{\alpha'},f_\alpha} \delta_{f_{\beta'},f_\beta} \\ & + \left\{ \frac{a_5}{2} + \frac{a_6}{2} - a_7 \right\} (\delta_{m_{\alpha'},m_\alpha} \delta_{m_{\beta'},-m_\beta} \delta_{f_{\alpha'},f_\alpha} \delta_{f_{\beta'},-f_\beta} \end{aligned}$$

$$+\delta_{m_{\alpha'},-m_\alpha}\delta_{m_{\beta'},m_\beta}\delta_{f_{\alpha'},-f_\alpha}\delta_{f_{\beta'},f_\beta})$$
$$+\frac{a_2}{2}\delta_{m_{\alpha'},-m_\alpha}\delta_{m_{\beta'},-m_\beta}\delta_{f_{\alpha'},-f_\alpha}\delta_{f_{\beta'},-f_\beta}$$
$$B_{\alpha'\beta',\alpha\beta}=b;\quad \text{for all } (m,f). \tag{10}$$

where $\alpha=m_\alpha,f_\alpha$, $\beta=m_\beta,f_\beta$, etc. Every RPA excitation $|n\rangle=\Gamma_n^\dagger|\text{RPA}\rangle$, with

$$\Gamma_n^\dagger=\sum_{\alpha\beta}(X^n_{\alpha\beta}\gamma^\dagger_{\alpha\beta}-Y^n_{\alpha\beta}\gamma_{\beta\alpha}) \tag{11}$$

and $\gamma^\dagger_{m_\alpha f_\alpha m_\beta f_\beta}=C^\dagger_{2m_\alpha f_\alpha}C_{1m_\beta f_\beta}$, is characterized by two amplitudes $X^n_{\alpha\beta}$ and $Y^n_{\alpha\beta}$ indicating the creation and annihilation of a pair, respectively. The amplitude-squares $|X^n_{\alpha\beta}|^2$ and $|Y^n_{\alpha\beta}|^2$ are analyzed in the next section in order to study the flavor content of each RPA-eigenstate.

4. RPA Results and the Analysis of the Wave Functions

In this section, we present the RPA results for the FSBH of Eq. (9). The implementation of the RPA-method will allow us to explore more in detail the structure of the pion state in terms of the interactions and to visualize it as a Goldstone boson on more involved effective QCD Hamiltonians like the one of Eq. (3). We have performed several fits of the parameters introduced in the previous section and four sets of values were selected as representative of different possible scenarios. On these examples, we shall illustrate on how to identify physical states using their quark content.

In Table 1, we list four set of parameters of the Hamiltonian of Eq. (9) and the corresponding RPA-eigenvalues at $b=b_{\text{fit}}$. The calculations shown in Table 1 were performed by following a simple procedure. The parameters ϵ_f and $\{a_i\}$ are chosen in order to get for $b=0$ (which is the TDA limit) energies within the range of 350–1100 MeV. Within this range of energies are located the physical mesons with negative parity, i.e., pseudo-scalar $(K(493),\eta(547.8),\eta'(957.7))$ and vector $(\rho(770),\omega(782),K^*(892),\phi(1020))$ mesons, which we attempt to describe as RPA excitations. We then study how they modify as $b\neq 0$, and finally, the $b=b_{\text{fit}}$ value is obtained when the lowest RPA-excitation approaches the energy of the pion mass ($\approx$ 150–200 MeV). It is worth to mention that we are not fitting the RPA solutions to experimental values since we do not know *a priori* the flavor content of the RPA solutions. Instead, we chose several scenarios (well established gaps between the TDA solutions) in order to study the effects of the ground state correlations.

These results in the domain $0\leq b\leq b_{\text{fit}}$ are shown in Fig. 2. We use a flavor dependent single particle term $\epsilon_f=m_{u,d}\delta_{f,-\frac{1}{2}}+m_s\delta_{f,\frac{1}{2}}$. Since we are not making any difference between up (u) and down (d) quarks, $f=-\frac{1}{2}$ will be used for both flavors and $f=\frac{1}{2}$ for strange quarks. To implement this flavor symmetry breaking term without changing the SO(4) structure of Eq. (4) we just added a flavor index to each operator, $C^\dagger_{\sigma m}\rightarrow C^\dagger_{\sigma m,f}$ with $m,f=\pm\frac{1}{2}$. Once this is done we are no

Table 1. Fit of parameters and the calculated RPA energies $E_i(\Omega_i)$[MeV]. Each of the states with energy E_i is Ω_i-folded.

Set	a_1	a_2	a_3	a_5	a_6	a_7	$b_{\rm fit}$	$E_1(1)$	$E_2(3)$	$E_3(1)$	$E_4(\Omega_4)$	$E_5(\Omega_5)$	$E_6(1)$	$E_7(3)$
1	100	50	200	−300	100	−150	45.00	184.81	579.10	716.44	780.00(4)	827.55(3)	1011.01	1033.34
2	100	100	200	0	50	−50	58.12	164.49	590.31	670.06	780.00(4)	863.27(3)	965.95	1086.41
3	100	−100	200	0	100	−150	54.37	187.27	364.98	402.11	735.12(3)	780.00(4)	895.17	1039.89
4	100	150	200	0	0	0	54.37	201.37	622.56	741.59	780.00(4)	930.00(3)	1042.88	1087.43

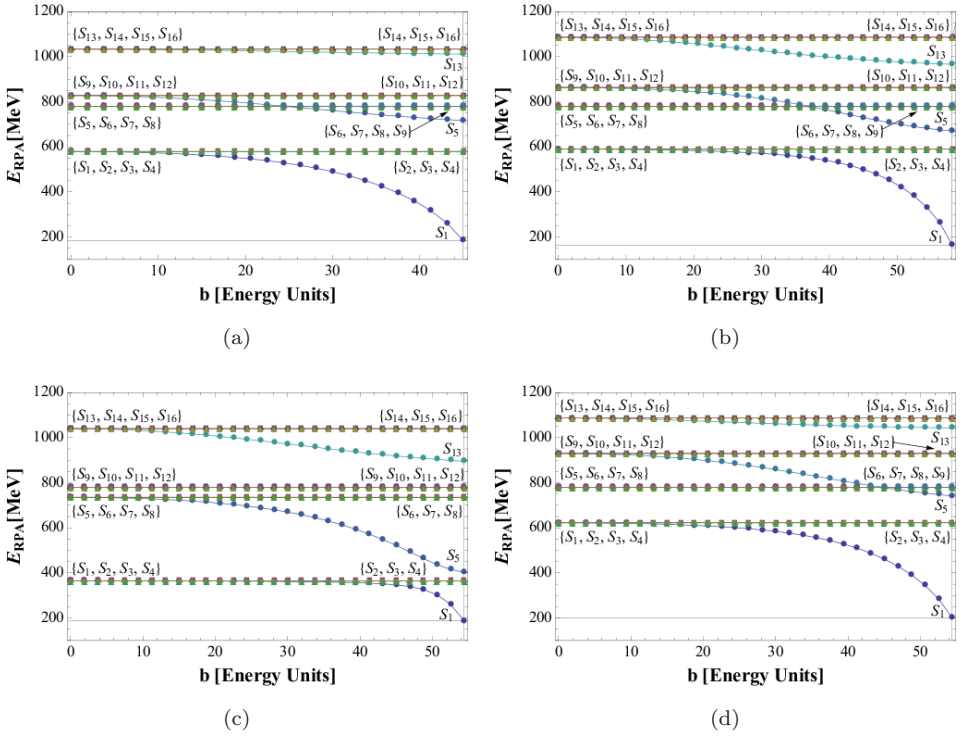

Fig. 2. Energy dependence of the RPA states, as a function of the backward-going matrix element, (b), for (a) Set-1, (b) Set-2, (c) Set-3 and (d) Set-4. The values of the parameters are given in Table 1.

longer working with a SU(3) flavor symmetry, and instead we have a (2+1)-flavor model. The RPA-solutions for the FSBH will be compared with the experimental data[32] in the following subsections.

To obtain the eigenvalues $E_i(\Omega_i)$ shown in Table 1, we have used effective quark masses $m_{u,d} = 80\,\text{MeV}$ and $m_s = 300\,\text{MeV}$. These masses exhibit explicitly that the chiral symmetry is broken. However, these values are lower compared to those used in quark models. In Ref. 30, it was argued that the reason for such lower values could be an indication that a more correlated ground state is needed and the RPA method was proposed. Here in our SO(4)-QCD-approach, the use of the RPA method allows us for constructing, quoting Ref. 30, a "more sophisticated ground state". The origin of these effective quark masses from the theory of QCD is related to the confinement of color charged particles as well as mass corrections due to interactions. Lattice calculations and the treatments based on Dyson–Schwinger equations of quark propagators have determined a saturation point for the quarks masses at small momentum ($p \to 0$).[13,14]

4.1. *Analysis of the RPA-states*

Since in Eq. (11) the indices (α, β) span a space of 16 configurations each RPA (or TDA) phonon state is a linear combination of these 16 states. When the backward-going amplitudes are set at $b = 0$ for all (α, β)-pairs (TDA-limit), one gets four energy eigenvalues each of them fourth-degenerated. These eigenvalues are shown in Fig. 2 (values at $b = 0$). Calling S_i $(i = 1, \ldots, 16)$ the phonon states, we group them in four subsets $\{S_1, S_2, S_3, S_4\}$, $\{S_5, S_6, S_7, S_8\}$, $\{S_9, S_{10}, S_{11}, S_{12}\}$ and $\{S_{13}, S_{14}, S_{15}, S_{16}\}$, each subset corresponding to an energy eigenvalue in the TDA limit. This is done in order to follow the evolution of the amplitudes $X^n_{\alpha\beta}$ and $Y^n_{\alpha\beta}$ of each RPA-excitation as a function of b until the point $b = b_{\text{fit}}$, which is the value associated to the collapse of the lowest RPA state close to the pion mass. By comparing the difference of the amplitudes $|X_{\alpha\beta}|^2 - |Y_{\alpha\beta}|^2$ for $b = 0$ and $b = b_{\text{fit}}$, we have extracted their quark–antiquark flavor content. Since we are not making any difference between u- and d-quark-masses, we denote from now on $q = u, d$ for up and down and s for strange quarks.

We analyze the RPA-states of each set of Fig. 2 for $b = 0$ and for $b = b_{\text{fit}}$. As we already mentioned before for $b = 0$ each state is four-fold degenerated while the degeneration of the RPA-states at b_{fit} (indicated by Ω_i in Table 1) is explicitly

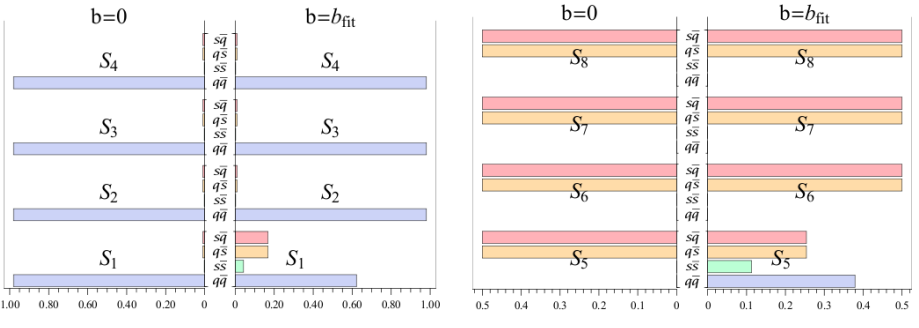

Fig. 3. $(X^2 - Y^2)$ amplitude analysis of $\{S_1, \ldots, S_4\}$ and $\{S_5, \ldots, S_8\}$ RPA-states of Set-1 at $b = 0$ and at $b = b_{\text{fit}}$.

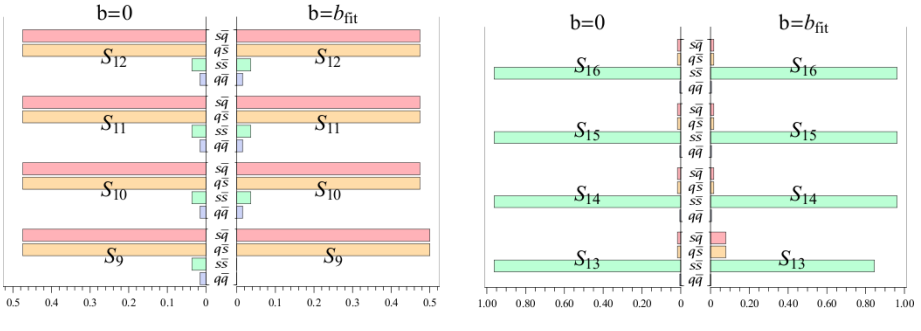

Fig. 4. $(X^2 - Y^2)$ amplitude analysis of $\{S_9, \ldots, S_{12}\}$ and $\{S_{13}, \ldots, S_{16}\}$ RPA-states of Set-1 at $b = 0$ and at $b = b_{\text{fit}}$.

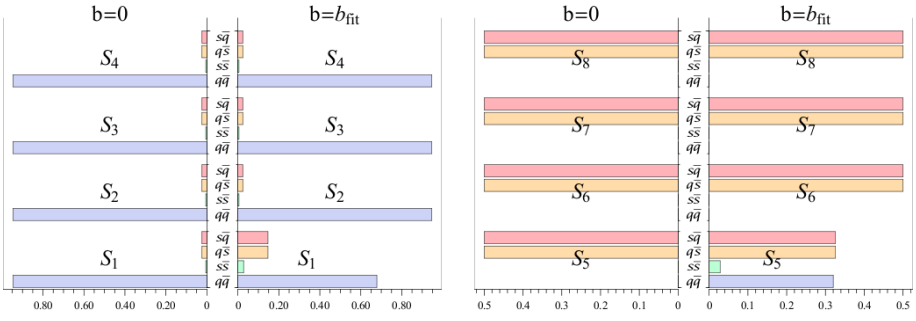

Fig. 5. Same as in Fig. 3 for Set-2.

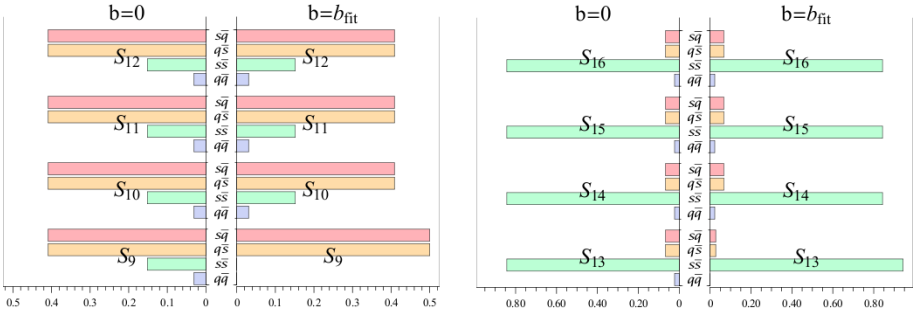

Fig. 6. Same as in Fig. 4 for Set-2.

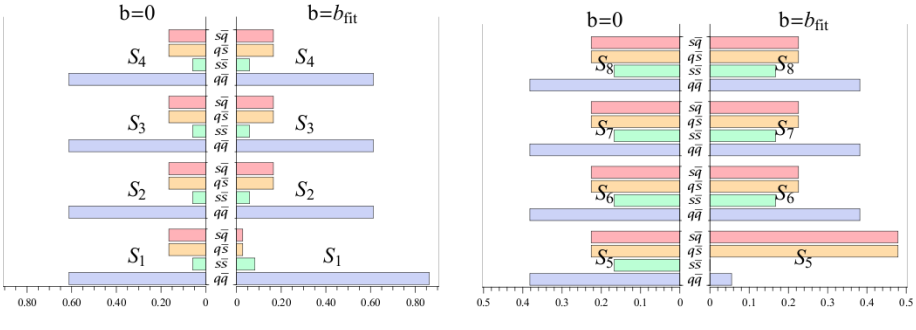

Fig. 7. Same as in Fig. 3 for Set-3.

shown on the right-hand side of each plot of Fig. 2 and will depend on the specific parametrization of the interaction. Therefore, we have sixteen states to analyze in order to look for the structure of physical states within the FSBH-SO(4) model. This search depends on the possibility of opening or closing specific flavor components. This is done in order to determine the flavor character and energy associated to each state.

In the following, we shall discuss the flavor content of each eigenstate obtained with the four set of parameters $\{a_i\}$ listed in Table 1, for both the TDA-limit at $b =$

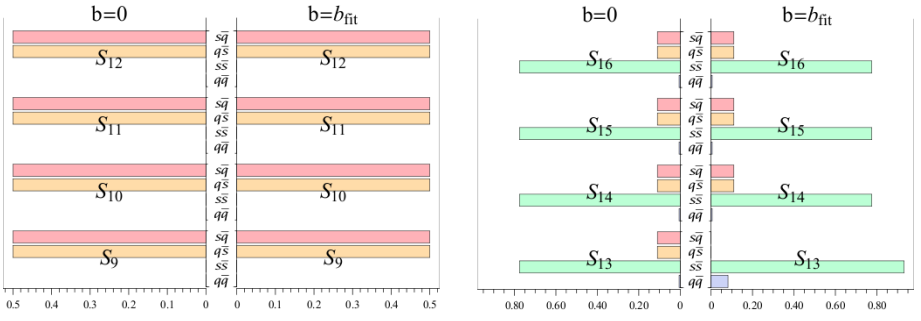

Fig. 8. Same as in Fig. 4 for Set-3.

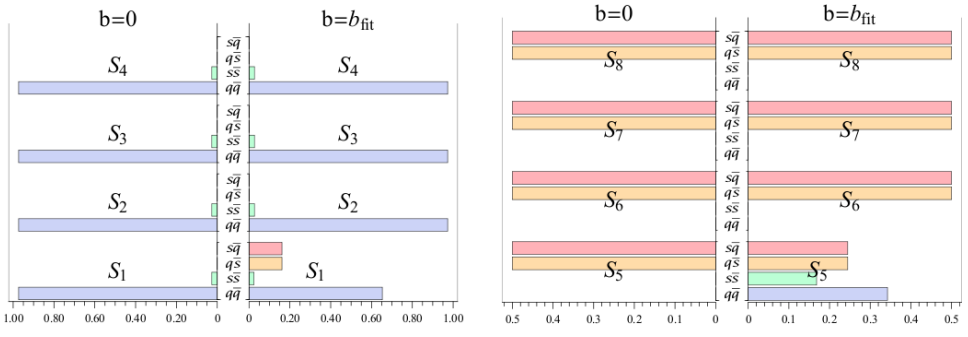

Fig. 9. Same as in Fig. 3 for Set-4.

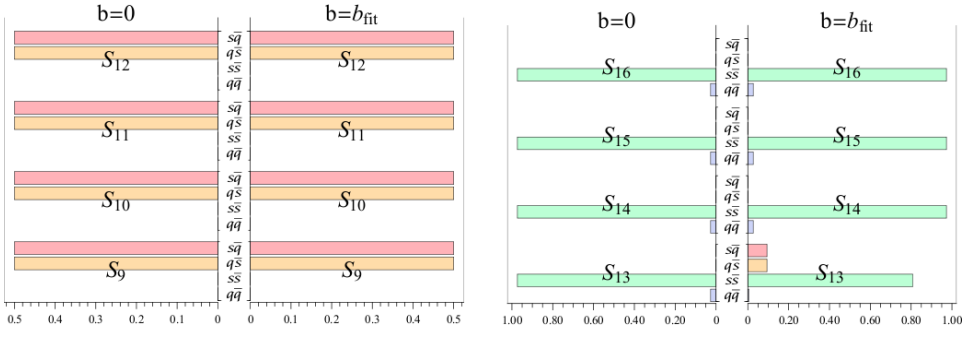

Fig. 10. Same as in Fig. 4 for Set-4.

0 and for the RPA-states at $b = b_{\rm fit}$. In Figs. 3–10 we show the $X^2 - Y^2$ amplitudes for each state. The flavor content $(q\bar{q}, s\bar{s}, q\bar{s}, s\bar{q})$ of each state is indicated by bar-charts for both $b = 0$ and $b = b_{\rm fit}$. The summation of all flavor-content-amplitudes is the normalization of the state. The detailed numerical analysis of the flavor content of each state is shown in Tables B.1–B.4 in Appendix B. The interpretation

of these states in terms of physical states is given in the text accompanying Figs. 3–10.

4.2. *Analysis of the parameter set-*1 (*Set-*1)

For the first set of parameters $\{a_i\}$ of Table 1 at $b = 0$ (TDA-limit) the results show that the flavor content of the $\{S_1, \ldots, S_4\}$-states is almost pure $q\bar{q}$, for the $\{S_5, \ldots, S_8\}$- and $\{S_9, \ldots, S_{12}\}$-states it is pure or almost pure $q\bar{s}, s\bar{q}$, and for the $\{S_{13}, \ldots, S_{16}\}$-states almost pure $s\bar{s}$, (see Figs. 3 and 4). The identification of the S_i-states with physical states at $b = 0$ is straightforward, except for states like η and η', since these states rely on nontrivial flavor mixing effects.[33–35] We do not implement traditional SU(3) flavor mixing since we have accounted for it within the $\{a_i\}$- and b-parameters, as it can be seen in the structure of the forward and backward matrices of Eq. (10) and quantified explicitly in Tables B.1–B.4 in Appendix B.

At $b = b_{\rm fit}$ we observe few relevant changes: The decrease of the energy of the first RPA excited state to 184.81 MeV (Fig. 2(a)), the considerable enhancement of the $q\bar{s}, s\bar{q}$- and the small contribution of $s\bar{s}$-components. The interpretation of this state as a collective state rises immediately, although the state S_1 continues to exhibit a $q\bar{q}$-dominance. These properties allow us to make our first guess of the physical pion state, $\pi(139)$, to be the collective state S_1. This interpretation might not be the natural one for the pion due to the considerable $q\bar{s}, s\bar{q}$ content, but within this parametrization the high collectivity of the S_1 state seems to be responsible for pushing downwards the RPA S_1 state of about 400 MeV respect the TDA solution. This is important to remark in order to get some insights about the structure of the pion state in phenomenological models and to look for the origin of such collectivity in real QCD. All of these properties come explicitly from considering the ph-correlations in the vacuum of the theory.

The almost pure $q\bar{q}$ $S_2, \ldots, S_4$ states are the ρ, ω-like states for the Set-1 and they are located at 579.10 MeV which is relatively low compared to the physical $\rho(770)$- and $\omega(782)$-mesons. However, the ground state correlations have generated an energy gap of about 400 MeV between the pion-like state and the ρ, ω-like states. Due to the simplicity of the schematic model these results are a good starting point for later corrections, e.g., like improvements on the spin dependence of the parameters.

At $b = b_{\rm fit}$, the state S_5 changes drastically its flavor content giving approximately a 50% decrease of the $q\bar{s}, s\bar{q}$ components and the enhancement of the $q\bar{q}$- and $s\bar{s}$- components and consequently of the $q\bar{q} + s\bar{s}$ combination. Putting this observation in the context of excitations, though the state is not a pure $q\bar{q} + s\bar{s}$ state, we consider the possibility that the state S_5 could be interpreted as the η-like state and/or η' at 716.44 MeV. The rearrangement of the states of Set-1 at $b = b_{\rm fit}$ suggests that the state S_5 is the first excitation of the $q\bar{q} + s\bar{s}$ components and that it could be associated to the η-meson. This opens the question on the location of the η'-like state in these RPA results. Either it is an independent excitation or the S_5

state is a mixture of both η and η'. For this first parametrization, the answer looks unclear, making our best guess that η- and η'-like states are mixed and located at 716.44 MeV.

On the other hand, the $S_6, \ldots, S_{12}$ states are the RPA kaon-like states of Set-1 at about 780.00–827.55 MeV. The last feature observed is that the state S_{13} suffers a small decrease in its energy as well as in its $s\bar{s}$ content. Figure 4 shows that it is still a $s\bar{s}$ dominated state making the identification of the $S_{13}, \ldots, S_{16}$ states as the ϕ-like states located at about 1011.01–1033.34 MeV (see Table 1), which are in good agreement with the physical $\phi(1020)$-meson.

4.3. *Analysis of the parameter set-2 (Set-2)*

The second set of parameters $\{a_i\}$ of Table 1 at $b = 0$ (TDA-limit) shows for the first eight states $S_1, \ldots, S_8$ no considerable difference with respect to Set-1, but for the $S_9, \ldots, S_{16}$-states, considerable changes are observed. The $S_9, \ldots, S_{12}$-states are dominated by the $q\bar{s}, s\bar{q}$-sector while the contribution of the $q\bar{q} + s\bar{s}$ combination amounts to 18% (see Table B.2 in Appendix B). The $S_{13}, \ldots, S_{16}$-states are dominated by the $s\bar{s}$ sector, then within the RPA results, the ϕ-like states lie at about 1086.41 MeV. The $S_{13}, \ldots, S_{16}$-states contain a small percentage of $q\bar{q}$ suggesting a mixture of η'- and ϕ-like states as well as the possibility that the η' meson is built by $q\bar{q} + s\bar{s}$ contributions but being highly dominated by the strange sector.

The changes observed for Set-2, with respect to the Set-1, might be associated with the null contribution of the a_5-interaction-term. It is not difficult to trace the origin of this interaction from the QCD Hamiltonian. As it was mentioned in Sec. 3, the activation of this term requires the inclusion of other degrees of freedom, like gluons. In particular, the a_5-term corresponds to the creation and annihilation of a ph pair connected by an operator which changes the spin by one unit. A direct candidate to describe this interaction is one-gluon-exchange.

At $b = b_{\text{fit}}$, we observe that the first RPA excited state, S_1, is lowered to 164.49 MeV (see Fig. 2(b)) and that it is more collective with respect to the case $b = 0$ (see Fig. 5). The energy of this state is 20 MeV lower than the one obtained with Set-1. However, the state continues being of the $q\bar{q}$-type and therefore, it is interpreted as the π-like state of Set-2, with almost the same collectivity of the π-like state of Set-1. The $S_2, \ldots, S_4$ states, which are almost pure $q\bar{q}$ states, remain at 590.31 MeV making them best candidates for ρ- and ω-like states of this Set.

The second change observed at $b = b_{\text{fit}}$ (also noted for Set-1) is the enhancement on the $q\bar{q}$ with a small admixture of $s\bar{s}$ components for the state S_5 with about 35% decreasing on the $q\bar{s}-$ and $s\bar{q}$-components. Such signal is important since it opens the possibility for the identification of the η-like state at about 670.06 MeV and the identification of the η'-like state at higher energies, which seems encouraging due to the 86.5% content of the $q\bar{q} + s\bar{s}$ combination on $S_{14}, \ldots, S_{16}$ states (see Table B.2 in Appendix B). The latter leaves well-defined sets of kaon-like states

at 780 MeV and 863.27 MeV. The last change observed for Set-2 is that the state S_{13} has been enhanced in the $s\bar{s}$ sector and lowered approximately 120 MeV in energy, leading to our first guess about the η'-like state located at 965.95 MeV, which is a good result compared to the physical $\eta'(957.7)$ meson. This state shows that the interactions and the vacuum-ph-correlations are trying to separate it from the $S_{14}, \ldots, S_{16}$ states. This picture agrees with the results of Ref. 30 where only pseudo-scalar mesons seem to be affected by the RPA treatment. Nevertheless, from the analysis of the amplitudes, for this η'-like state, we see that the $s\bar{s}$ combination is dominant. The null contribution of the a_5 term in Set-2, seems to be related with the presence of larger $q\bar{q}$ content at higher energies, with respect to the results obtained with the parametrization of Set-1. The latter might suggest that a better interpretation of the η'-like state in this model could be related with the selection of the a_i parameters associated to those terms capable of flavor mixing, i.e., a_2, a_5, a_6, a_7 and b. The choice of values for the coefficients a_i and b is a sensible aspect at the time of making the calculations, since in principle they can be taken as free parameters, only restricted to satisfy that the TDA solutions lie within the range of 350–1100 MeV. However, we can analyze gradually the effects of the parameters in order to reproduce some observed features of the meson spectrum and explore the dependence of the results upon them.

Finally, the $S_{14}, \ldots, S_{16}$ states due to their $s\bar{s}$ dominant nature are identified with ϕ-like states at 1086.41 MeV, which is also a good estimation for the physical $\phi(1020)$ meson.

4.4. *Analysis of the parameter set-3 (Set-3)*

The results obtained with the Set-3 of parameters $\{a_i\}$ of Table 1 are interesting for several reasons: they exhibit a bigger gap between energies in the TDA-limit and the location of the first excited subset $S_1, \ldots, S_4$ is closer to the pion energy (see Fig. 2(c)). Despite these larger gaps in energies, most of the states look like mixtures.

At $b = 0$ several flavor sectors appear mixed up and only one subset remains pure in $q\bar{s}$ and $s\bar{q}$ configurations, (see Figs. 7 and 8). The $S_1, \ldots, S_4$-states are mostly admixtures between the $q\bar{q}$- and $q\bar{s}, s\bar{q}$-sectors, indicating that the most probable states involved would be π-, ρ-, ω- and kaon-like states. The $S_5, \ldots, S_8$-states show a high percentage of $q\bar{q}+s\bar{s}$ combinations which are even higher than the $q\bar{s}+s\bar{q}$ one (see Table B.3 in Appendix B) allowing the identification of η-like mesons within these states. The states $S_9, \ldots, S_{12}$ belong to the pure $q\bar{s}$- and $s\bar{q}$ sector indicating a clear identification of kaon-like states while the $S_{13}, \ldots, S_{16}$-states are $s\bar{s}$-dominated and they are directly associated with ϕ-like states. At $b = 0$, there is no signal of considerable percentage of $q\bar{q}$ contribution in the $S_9, \ldots S_{16}$, i.e., above 735.12 MeV (see Table B.3 in Appendix B).

At $b = b_{\text{fit}}$, we observe peculiar changes compared not only to $b = 0$ but also to the results previously analyzed for Set-1 and Set-2. The π-like state is found at 187.27 MeV and the decreasing of the $q\bar{s}$- and $s\bar{q}$-components is stronger. This

makes the identification of the π-like state of Set-3 more like a $q\bar{q}$-pair condensate, but it still shows some collectivity. The less collectivity of the π-like state of Set-3 with respect to those of Set-1 and Set-2 seems to be a consequence of the a_2 term, since it changes sign and therefore decreases the diagonal part of the forward matrix, Eq. (10). It also seems to allow more flavor mixing in the first subset $S_1, \ldots, S_4$ of the TDA solutions ($b = 0$). Then, when the ground state correlations, quantified by the backward-going term ($b \neq 0$) are activated, the system pushes the RPA S_1 state downwards by suppressing the $q\bar{s}$ and $s\bar{q}$ contents, which one can think as the natural description of the π-like state. Of course, the rearrangement of the other RPA S_i states would be different that those described by Set-1 and Set-2, as it is discussed in the following.

The second change observed in Set-3 at $b = b_{\text{fit}}$ is the enhancement on the $q\bar{s}$- and $q\bar{s}$-channels for the state S_5, which is also pushed downwards in energy almost to the energy of the $S_2, \ldots, S_4$-states, supporting our first guess (at $b = 0$) which included the presence of kaon-like states. Therefore, the energy range 364.98–402.11 MeV associated to the $S_2, \ldots, S_5$ states is considerable low for physical ρ, ω mesons but relatively good for pseudo-scalar kaons $K(493)$. This set also indicates that a better fit for the pseudo-scalar kaons can be obtained at the expenses of lowering the energies of the ρ- and ω-like states, and generating a smaller energy gap between the π-like state and the ρ, ω-like states.

The $S_6, \ldots, S_8$ states are dominated by the $q\bar{q} + s\bar{s}$-combination, with high probability of containing the η-like state at about 735.12 MeV. This energy is higher than the reported value $\eta(547.8)$ and it could be a consequence of the percentage of strange content in these states. The $S_9, \ldots, S_{12}$ states are not modified in their flavor content keeping their $q\bar{s}, s\bar{q}$ structure. They are located at 780 MeV and related to physical kaon states. The energy of these kaon-like states is relatively low with respect to $K^*(892)$. Because of these energy differences, one might question the model but it is worth to mention that our aim is to get some insights on the structure of the states and test the many-body methods and interactions in a reduced space (see Fig. 1) rather than performing a fit of every individual state.

The state S_{13} is pushed downwards in energy and it is considerable enhanced in the $q\bar{q} + s\bar{s}$ combination while its $q\bar{s}$- and $s\bar{q}$-components are suppressed (see Fig. 8). Then, the $q\bar{q}$ enhancement effect above 735.12 MeV is associated with the ph-correlations considered in the RPA-ground-state. These properties make the state S_{13} a good candidate to represent the η'-like state due to its location at energy 895.17 MeV. The latter is in relatively good agreement with the physical value $\eta'(957.7)$. We can compare the experimental energy difference $E_{\eta'} - E_{\eta} \approx 400$ MeV with the calculated energy difference $E_{S_{13}} - E_{S_7} = 160$ MeV, which is about one-half of the experimental value. In spite of the simplicity of the present model, Set-3 allows us to estimate the energy difference $E_{\eta'} - E_{\eta}$, something difficult to achieve in realistic QCD calculations.[33] The easier identification of the η'-like state in Set-3 seems to be related with the sign of the a_2-term, which also seems to be responsible for a higher $q\bar{s}$ and $s\bar{q}$ content in the TDA subset $S_{13}, \ldots, S_{16}$, and once again, the

effects of the ground state correlations evident in the RPA S_{13} state is to suppress the $q\bar{s}$ and $s\bar{q}$ content and push it downwards in energy.

Finally, $S_{14}, \ldots, S_{16}$-states are isolated at higher energies keeping their dominant $s\bar{s}$- sector untouched and therefore making them the best candidates to be the ϕ-like states at the energy 1039.89 MeV. This is in good agreement with the experimental value $\phi(1020)$.

4.5. *Analysis of the parameter set-4 (Set-4)*

The parametrization of Set-4 shows almost only pure states at $b = 0$ (see Figs. 9 and 10) where the states $\{S_1, \ldots S_4\}$ and $\{S_{13}, \ldots S_{16}\}$ are $q\bar{q}$ and $s\bar{s}$ dominated, respectively. The states $\{S_5, \ldots S_8\}$ and $\{S_9, \ldots S_{12}\}$ show equal amplitudes in the $q\bar{s}$ and $s\bar{q}$ sectors. This might be a consequence of the fact that most of the bilinear combinations $\hat{J}_i\hat{V}_j$ with $i \neq j$, do not play any role in the interaction, see Eq. (9) and Table 1. This Set is also a good test for the effects of ph-correlations coming from the vacuum state for $b = b_{\text{fit}}$ without the influence of additional flavor mixtures.

At $b = b_{\text{fit}}$, the first RPA excitation is located at 201.37 MeV (see Fig. 2(d)) breaking its almost pure content by a more collective one (see Table B.4 in Appendix B). However, this state keeps its $q\bar{q}$ content dominant, representing the π-like state of Set-4 (very similar to the π-like states of Set-1 and Set-2). The remaining $q\bar{q}$ dominated $S_2, \ldots, S_4$ states, identified as ρ- and ω-like states, lie at energy 622.56 MeV. This is encouraging for further corrections in order to get closer to the reported values $\rho(770)$ and $\omega(782)$.

The state S_5 is an explicit signal of $q\bar{q} + s\bar{s}$ excitations and it lies at 741.59 MeV. This is the only state below 800 MeV with dominant $q\bar{q} + s\bar{s}$ combination and with more than 10% of $s\bar{s}$ content. Therefore, its identification with a η-like state seems reasonable. There is also some room to think of the S_5 state as a mixture of the η- and η'-like states, just like in the case of Set-1. However, for Set-4, there is about 3% of $q\bar{q}$ content in the higher subset $S_{13}, \ldots, S_{16}$, which did not appear in the case of Set-1. Therefore, we could think about two possible scenarios for the identification of the η'-like state for the parametrization of Set-4, which we discuss below.

The two subsets of kaon-like $S_6, \ldots, S_8$- and $S_9, \ldots, S_{12}$-states are located at 780 and 930 MeV, respectively.

The state S_{13} is located at 1042.88 MeV. This state decreases its energy about 40 MeV with respect to the $S_{14}, \ldots, S_{16}$ states. This indicates that the effects of the interactions and the ph-correlations of the vacuum are not able to create a bigger energy separation. For the Set-2 and Set-3 the energy separation between the RPA S_{13} state and the $S_{14}, \ldots, S_{16}$ states was about 120 and 150 MeV, respectively. Without such separation, it seems that the Set-4 could present two possible scenarios for the η'-like state. In the first scenario, the η- and η'-like states are mixed and located at 741.59 MeV, which is almost the average energy of the physical $\eta(547.8)$ and $\eta'(957.7)$ states. Leading to the identification of the $s\bar{s}$ dominated states $S_{13}, \ldots, S_{16}$ as the ϕ-like states. The second scenario is based on the fact that

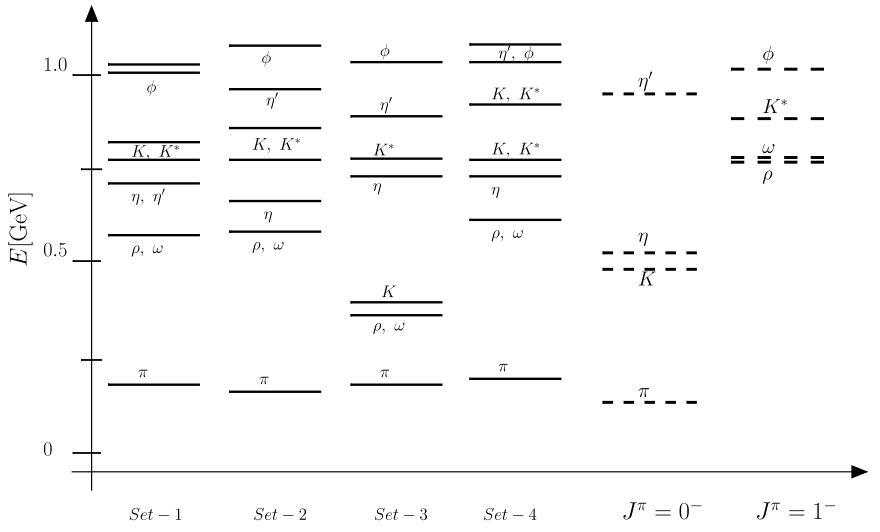

Fig. 11. RPA solutions for Sets$-1, 2, 3, 4$ (solid-lines) and experimental pseudo-scalar ($J^\pi = 0^-$) and vector mesons ($J^\pi = 1^-$) up to 1 GeV (dashed-lines). The labeling of the calculated RPA states follows from the analysis of their flavor content.

the interactions and the ground state correlations were not capable of extracting the η'-like state from the subset $S_{13}, \ldots, S_{16}$. Thus, the η'- and ϕ-like states remain mixed up and located within the range of energy 1042.88–1087.43 MeV.

The latter identification provides a possible scenario for the model which describes the η-like meson as a very collective state built by a $q\bar{q}$ content almost twice the $s\bar{s}$ one and where the combinations $q\bar{q} + s\bar{s}$ and $q\bar{s} + s\bar{q}$ have almost the same weight. This is not the case of the η'-meson, which is built as a nearly pure $s\bar{s}$ state. This description might be naive referring to a theory like QCD, but for this simple model it could be a reasonable explanation for the difference in energy between the η- and η'-mesons.

The possibility that the η'-like state could be mixed up with the ϕ-like states within the $S_{13}, \ldots, S_{16}$ states, allow us to quantify the energy difference $\frac{E_{S_{13}}+E_{S_{14}}}{2} - E_{S_5} = 323.56$ MeV, which is a good estimation for the experimental value $E_{\eta'} - E_\eta \approx 400$ MeV.

Finally, in Fig. 11, we collect the results of the RPA calculations performed with the parameters of Set-1–Set-4, and compare them with the available data. In Fig. 11, for the states obtained with the parametrization of Set-4, the state shown as the η'-like state is the one described by the second scenario of Set-4, as explained before. The first scenario of Set-4 is very similar to that depicted by Set-1.

5. Summary

In this work, we have studied the SO(4) group structure contained in the QCD Hamiltonian written in the canonical Coulomb gauge representation. The SO(4)

group seems to host a significant number of features associated to the low-energy QCD mesons. We have also extended our previous study[28] of the SO(4) group structure to include *ph*-like correlations in the ground state. This was done by means of the RPA and taken into account the broken SU(3)-flavor-symmetry. Both the inclusion of *ph*-correlations in the ground state and the broken flavor symmetry represented by a flavor dependent single particle term improve significantly the agreement with data, as compared to the results of Ref. 28.

Relevant features were observed in the calculated RPA spectrum for each set of parameters:

- The state S_1 with dominant $q\bar{q}$-content is lowered significantly in energy. Particularly, the best representation of the pion within this work is by the S_1 state, as a collective state lying at about 200 MeV.
- The ρ, ω-like states are consistently lower than the experimental values. This leaves room for further spin-dependent corrections of the coefficients.
- The state S_5 is also lowered in energy by the effects of *ph*-correlations on the ground state. It is a good example to illustrate the effects of the backward-going term at higher energies, by the activation or suppression of flavor contents. With the representative RPA results presented in Sec. 4, we were able to get some insights about the structure of the pseudo-scalar η- and kaon-states by analyzing the state S_5.
- The identification of kaon- and ϕ-like states is straightforward within our RPA results. Their associated energies are reasonable compared to data.
- The effects of the *ph*-correlations of the ground state over the states at about 1 GeV can still be quantified by changes in theirs flavor content and energy. This led to our best identification of the η'-like state at about 895.17 MeV.

In general, these considerations allowed us to make a more realistic guess about the presence of physical meson states. As shown here, we have started from a rigorously-formulated QCD Hamiltonian, mapped it onto a group representation and found that the masses of physical states at about 1 GeV are in correspondence with the eigenvalues predicted by our RPA treatment of the SO(4)-group-QCD Hamiltonian. The use of these concepts may lead us to a better understanding of the structure of physical states belonging to the QCD scheme. We conclude our analysis by stressing the potential of the use of standard many-body techniques to explore the extremely rich and complicated structure of QCD in the nonperturbative regime.

Acknowledgments

One of the authors (T.Y.-M.) thanks the National Research Council of Argentina (CONICET) for a post-doctoral scholarships. O.C. is a member of the scientific career of the CONICET. P.O.H acknowledges financial help from DGAPA-PAPIIT

(IN100315) and from CONACYT (Mexico, grant No. 251817). This work has been supported financially by the CONICET (PIP-282) and the ANPCYT of Argentina.

Appendix A. RPA Procedure

The RPA method can be seen as a direct extension of the TDA method where the collective ph-operator is written as

$$\hat{\Gamma}_n^\dagger = \sum_{m_\alpha m_\beta} X^n_{m_\alpha m_\beta} \gamma^\dagger_{m_\alpha m_\beta} \tag{A.1}$$

with $\gamma^\dagger_{m_\alpha m_\beta} = C^\dagger_{2m_\alpha} C_{1m_\beta}$, which restricts the approximation to the space of $1p-1h$ excitations relevant for low-lying states of negative parity. The nth TDA-excited state is given by $|n\rangle = \hat{\Gamma}^\dagger_n|\tilde{0}\rangle$ and the ground state satisfies $\Gamma_n|\tilde{0}\rangle = 0$.

The TDA-equation of motion is written as

$$\sum_{m_\alpha m_\beta} \langle\tilde{0}|[\gamma_{m_{\beta'} m_{\alpha'}}, [\hat{H}, \gamma^\dagger_{m_\alpha m_\beta}]]|\tilde{0}\rangle X^n_{m_\alpha m_\beta} = E_n^{TD} X^n_{m_{\alpha'} m_{\beta'}}, \tag{A.2}$$

where the $1p-1h$ correlations are only taken into account in the excited states keeping the ground state $|\tilde{0}\rangle$ unchanged.

The most straightforward generalization of the collective $1p-1h$-operator, and the corresponding excitations, is the RPA. Calling $|\mathrm{RPA}\rangle$ the correlated ground state and defining the phonon operator as

$$\Gamma^\dagger_n = \sum_{m_\alpha m_\beta} (X^n_{m_\alpha m_\beta} \gamma^\dagger_{m_\alpha m_\beta} - Y^n_{m_\alpha m_\beta} \gamma_{m_\beta m_\alpha}), \tag{A.3}$$

with $\gamma_{m_\beta m_\alpha} = (\gamma^\dagger_{m_\alpha m_\beta})^\dagger$, the nth-RPA-state is constructed as $|n\rangle_{\mathrm{RPA}} = \Gamma^\dagger_n|\mathrm{RPA}\rangle$. The RPA-ground-state is constructed in such a way that the condition $\Gamma_n|\mathrm{RPA}\rangle = 0$ is fulfilled.

The equation of motion ($H|n\rangle = E_n^{\mathrm{RPA}}|n\rangle$) in the RPA formalism is equivalent to the double commutator

$$\langle\mathrm{RPA}|[\hat{\Gamma}_{n'}, [H, \hat{\Gamma}^\dagger_n]]|\mathrm{RPA}\rangle = E_n^{\mathrm{RPA}} \delta_{n,n'}, \tag{A.4}$$

with eigenvalues E_n^{RPA}. Therefore, from Eq. (A.4), we get two sets of equations, which in matrix form can be written as

$$\begin{pmatrix} A & B \\ B^* & A^* \end{pmatrix} \begin{pmatrix} X^n \\ Y^n \end{pmatrix} = E_n^{\mathrm{RPA}} \begin{pmatrix} 1 & 0 \\ 0 & -1 \end{pmatrix} \begin{pmatrix} X^n \\ Y^n \end{pmatrix}, \tag{A.5}$$

with

$$\begin{aligned} A_{\alpha'\beta',\alpha\beta} &= \langle\tilde{0}|[C^\dagger_{1\beta'} C_{2\alpha'}, [H, C^\dagger_{2\alpha} C_{1\beta}]]|\tilde{0}\rangle, \\ B_{\alpha'\beta',\alpha,\beta} &= \langle\tilde{0}|[C^\dagger_{1\beta'} C_{2\alpha'}, [H, C^\dagger_{1\beta} C_{2\alpha}]]|\tilde{0}\rangle, \end{aligned} \tag{A.6}$$

being the forward and backward matrices of the RPA-method, respectively.

To calculate the commutators in Eq. (A.6), we enforce the *quasi–boson* approximation

$$\langle\mathrm{RPA}|[C^\dagger_{1\beta'} C_{2\alpha'}, C^\dagger_{2\alpha} C_{1\beta}]|\mathrm{RPA}\rangle \simeq \langle\tilde{0}|[C^\dagger_{1\beta'} C_{2\alpha'}, C^\dagger_{2\alpha} C_{1\beta}]|\tilde{0}\rangle = \delta_{\alpha'\alpha}\delta_{\beta'\beta}. \tag{A.7}$$

Appendix B. Flavor Content of the RPA Solutions

In this appendix, and for the sake of completeness, we are listening the amplitudes of the $q\bar{q}, s\bar{s}, q\bar{s}$ and $s\bar{q}$ configurations of the TDA ($b = 0$) and RPA ($b = b_{\rm fit}$) phonon states (see Sec. 4), for the different sets of parametrization considered in the calculations.

Table B.1. $(X^2 - Y^2)-$RPA-amplitudes, in percentage, in terms of the flavor content of each state of Set-1.

Content\ S_k states	S_1	S_2	S_3	S_4	S_5	S_6	S_7	S_8	S_9	S_{10}	S_{11}	S_{12}	S_{13}	S_{14}	S_{15}	S_{16}
$b = 0$																
$q\bar{q}$	98.0	98.0	98.0	98.0	0.0	0.0	0.0	0.0	1.5	1.5	1.5	1.5	0.4	0.4	0.4	0.4
$s\bar{s}$	0.2	0.2	0.2	0.2	0.0	0.0	0.0	0.0	3.6	3.6	3.6	3.6	96.2	96.2	96.2	96.2
$q\bar{s}$	0.9	0.9	0.9	0.9	50.0	50.0	50.0	50.0	47.4	47.4	47.4	47.4	1.6	1.6	1.6	1.6
$s\bar{q}$	0.9	0.9	0.9	0.9	50.0	50.0	50.0	50.0	47.4	47.4	47.4	47.4	1.6	1.6	1.6	1.6
$b = b_{\rm fit}$																
$q\bar{q}$	62.2	98.0	98.0	98.0	37.9	0.0	0.0	0.0	0.0	1.5	1.5	1.5	−0.1	0.4	0.4	0.4
$s\bar{s}$	4.2	0.2	0.2	0.2	11.3	0.0	0.0	0.0	0.0	3.6	3.6	3.6	84.4	96.2	96.2	96.2
$q\bar{s}$	16.7	0.9	0.9	0.9	25.4	50.0	50.0	50.0	50.0	47.4	47.4	47.4	7.8	1.6	1.6	1.6
$s\bar{q}$	16.7	0.9	0.9	0.9	25.4	50.0	50.0	50.0	50.0	47.4	47.4	47.4	7.8	1.6	1.6	1.6

Table B.2. Same as in Table B.1 for Set-2.

Content\ S_k states	S_1	S_2	S_3	S_4	S_5	S_6	S_7	S_8	S_9	S_{10}	S_{11}	S_{12}	S_{13}	S_{14}	S_{15}	S_{16}
$b = 0$																
$q\bar{q}$	94.6	94.6	94.6	94.6	0.0	0.0	0.0	0.0	3.0	3.0	3.0	3.0	2.3	2.3	2.3	2.3
$s\bar{s}$	0.5	0.5	0.5	0.5	0.0	0.0	0.0	0.0	15.1	15.1	15.1	15.1	84.3	84.3	84.3	84.3
$q\bar{s}$	2.4	2.4	2.4	2.4	50.0	50.0	50.0	50.0	40.8	40.8	40.8	40.8	6.7	6.7	6.7	6.7
$s\bar{q}$	2.4	2.4	2.4	2.4	50.0	50.0	50.0	50.0	40.8	40.8	40.8	40.8	6.7	6.7	6.7	6.7
$b = 58.12$																
$q\bar{q}$	67.8	94.6	94.6	94.6	32.0	0.0	0.0	0.0	0.0	3.0	3.0	3.0	0.1	2.3	2.3	2.3
$s\bar{s}$	2.8	0.5	0.5	0.5	2.8	0.0	0.0	0.0	0.0	15.1	15.1	15.1	94.3	84.3	84.3	84.3
$q\bar{s}$	14.6	2.4	2.4	2.4	32.5	50.0	50.0	50.0	50.0	40.8	40.8	40.8	2.7	6.7	6.7	6.7
$s\bar{q}$	14.6	2.4	2.4	2.4	32.5	50.0	50.0	50.0	50.0	40.8	40.8	40.8	2.7	6.7	6.7	6.7

Table B.3. Same as in Table B.1 for Set-3.

Content\ S_k states	S_1	S_2	S_3	S_4	S_5	S_6	S_7	S_8	S_9	S_{10}	S_{11}	S_{12}	S_{13}	S_{14}	S_{15}	S_{16}
$b = 0$																
$q\bar{q}$	61.2	61.2	61.2	61.2	38.2	38.2	38.2	38.2	0.0	0.0	0.0	0.0	0.5	0.5	0.5	0.5
$s\bar{s}$	5.8	5.8	5.8	5.8	16.7	16.7	16.7	16.7	0.0	0.0	0.0	0.0	77.5	77.5	77.5	77.5
$q\bar{s}$	16.4	16.4	16.4	16.4	22.5	22.5	22.5	22.5	50.0	50.0	50.0	50.0	10.9	10.9	10.9	10.9
$s\bar{q}$	16.4	16.4	16.4	16.4	22.5	22.5	22.5	22.5	50.0	50.0	50.0	50.0	10.9	10.9	10.9	10.9

Table B.3. (*Continued*)

Content\ S_k states	S_1	S_2	S_3	S_4	S_5	S_6	S_7	S_8	S_9	S_{10}	S_{11}	S_{12}	S_{13}	S_{14}	S_{15}	S_{16}
								$b = 54.37$								
$q\bar{q}$	86.3	61.2	61.2	61.2	5.0	38.2	38.2	38.2	0.0	00.0	0.0	0.0	8.1	0.5	0.5	0.5
$s\bar{s}$	8.2	5.8	5.8	5.8	0.0	16.7	16.7	16.7	0.0	0.0	0.0	0.0	93.1	77.5	77.5	77.5
$q\bar{s}$	2.7	16.4	16.4	16.4	47.5	22.5	22.5	22.5	50.0	50.0	50.0	50.0	−0.6	10.9	10.9	10.9
$s\bar{q}$	2.7	16.4	16.4	16.4	47.5	22.5	22.5	22.5	50.0	50.0	50.0	50.0	−0.6	10.9	10.9	10.9

Table B.4. Same as in Table B.1 for Set-4.

Content\ S_k states	S_1	S_2	S_3	S_4	S_5	S_6	S_7	S_8	S_9	S_{10}	S_{11}	S_{12}	S_{13}	S_{14}	S_{15}	S_{16}
								$b = 0$								
$q\bar{q}$	97.3	97.3	97.3	97.3	0.0	0.0	0.0	0.0	0.0	0.0	0.0	0.0	2.7	2.7	2.7	2.7
$s\bar{s}$	2.7	2.7	2.7	2.7	0.0	0.0	0.0	0.0	0.0	0.0	0.0	0.0	97.3	97.3	97.3	97.3
$q\bar{s}$	0.0	0.0	0.0	0.0	50.0	50.0	50.0	50.0	50.0	50.0	50.0	50.0	0.0	0.0	0.0	0.0
$s\bar{q}$	0.0	0.0	0.0	0.0	50.0	50.0	50.0	50.0	50.0	50.0	50.0	50.0	0.0	0.0	0.0	0.0
								$b = 54.37$								
$q\bar{q}$	65.3	97.3	97.3	97.3	34.3	0.0	0.0	0.0	0.0	0.0	0.0	0.0	0.4	2.7	2.7	2.7
$s\bar{s}$	2.4	2.7	2.7	2.7	16.8	0.0	0.0	0.0	0.0	0.0	0.0	0.0	80.8	97.3	97.3	97.3
$q\bar{s}$	16.1	0.0	0.0	0.0	24.4	50.0	50.0	50.0	50.0	50.0	50.0	50.0	9.4	0.0	0.0	0.0
$s\bar{q}$	16.1	0.0	0.0	0.0	24.4	50.0	50.0	50.0	50.0	50.0	50.0	50.0	9.4	0.0	0.0	0.0

References

1. T. D. Lee, *Particle Physics and Introduction to Field Theory* (Science Press, 1988).
2. M. E. Peskin and D. V. Schroeder, *An Introduction to Quantum Field Theory* (Westview Press, 1995).
3. W. Greiner and J. Reinhardt, *Field Quantization* (Springer, 1996).
4. P. de Forcrand and M. D'Elia, *Phys. Rev. Lett.* **82** (1999) 4582.
5. A. P. Szczepaniak and E. S. Swanson, *Phys. Rev. D* **65** (2001) 025012.
6. R. Bijker and E. Santopinto, *J. Phys., Conf. Ser.* **578** (2015) 012015.
7. M. R. Pennington, *J. Phys., Conf. Ser.* **18** (2005) 173.
8. J. J. Dudek, R. G. Edwards and C. E. Thomas, *Phys. Rev. D* **79** (2009) 094504.
9. J. Dudek, *Phys. Rev. D* **84** (2011) 074023.
10. P. Guo, T. Yepez-Martinez and A. P. Szczepaniak, *Phys. Rev. D* **89** (2014) 116005.
11. C. D. Roberts and A. G. Williams, *Prog. Part. Nucl. Phys.* **33** (1994) 477.
12. R. Alkofer and L. von Smekal, *Phys. Rep.* **353** (2001) 281–465.
13. M. S. Bhagwat, M. A. Pichowsky, C. D. Roberts and P. C. Tandy, *Phys. Rev. C* **68** (2003) 015203.
14. C. S. Fischer and M. R. Pennington, *Phys. Rev. D* **73** (2006) 034029.
15. J. Engels, F. Karsch, H. Satz and I. Montvay, *Nucl. Phys. B* **205** (1982) 545.
16. G. Boyd *et al.*, *Nucl. Phys. B* **469** (1996) 419.
17. K. J. Juge, J. Kuti and C. J. Morningstar, *Nucl. Phys. B*, (*Proc. Suppl.*) **63** (1998) 326.
18. J. J. Dudek, R. G. Edwards and D. G. Richards, *Phys. Rev. D* **73** (2006) 074507.
19. G. Burgio, M. Quandt and H. Reinhardt, *Phys. Rev. Lett.* **102** (2009) 032002.

20. QCDSF-UKQCD Collab. (W. Bietenholz *et al.*), *Phys. Rev. D* **84** (2011) 054509.
21. A. Szczepaniak, E. S. Swanson, C.-R. Ji and S. R. Cotanch, *Phys. Rev. Lett.* **76** (1996) 2011.
22. C. Feuchter and H. Reinhardt, *Phys. Rev. D* **70** (2004) 105021.
23. P. O. Hess and A. P. Szczepaniak, *Phys. Rev. C* **73** (2006) 025201.
24. D. Epple, H. Reinhardt and W. Schleifenbaum, *Phys. Rev. D* **75** (2007) 045011.
25. T. Yepez-Martinez, P. O. Hess, A. P. Szczepaniak and O. Civitarese, *Phys. Rev. C* **81** (2010) 045204.
26. T. Yepez-Martinez, A. Amor, P. O. Hess, A. P. Szczepaniak and O. Civitarese, *Int. J. Mod. Phys. E* **20** (2011) 192–199.
27. T. Yepez-Martinez, D. A. Amor-Quiroz, P. O. Hess and O. Civitarese, *J. Phys. Conf. Ser.* **730** (2016) 012020.
28. T. Yepez-Martinez, O. Civitarese and P. O. Hess, *Int. J. Mod. Phys. E* **25** (2016) 1650067.
29. P. Ring and P. Schuck, *The Nuclear Many Body Problem* (Springer, Heidelberg, 1980).
30. F. J. Llanes-Estrada and S. R. Cotanch, *Phys. Rev. Lett.* **84** (2000) 1102.
31. A. Bohm, *Quantum Mechanics*: *Fundations and Applications* (Springer-Verlag, 1979).
32. Particle Data Group (C. Patrignani *et al.*), *Chin. Phys. C* **40** (2016) 100001.
33. J. J. Dudek *et al.*, *Phys. Rev. D* **83** (2011) 111502(R).
34. F.-G. Cao, *Phys. Rev. D* **85** (2012) 057501.
35. T. N. Pham, *Phys. Rev. D* **92** (2015) 054021.